TESTS AND PERFORMANCE EVALUATION OF DMC IMAGES AND NEW METHODS FOR THEIR PROCESSING

Li Zhang [a,1], Sultan Kocaman [a], Devrim Akca [a], Wolfgang Kornus [b], Emmanuel Baltsavias [a, *]
[a] Institute of Geodesy and Photogrammetry, ETH Zurich,
CH-8093, Zurich, Switzerland - (devrim, skocaman, manos)@geod.baug.ethz.ch, zhangl@casm.ae.cn
[b] Cartographic Institute of Catalonia (ICC), Parc de Montjuïc, 08038 Barcelona, Spain - wkornus@icc.es

WG I/4 Airborne digital photogrammetric sensor systems

KEY WORDS: Aerial digital cameras, DMC, Sensor modelling, Triangulation, Digital Surface Models, Accuracy analysis

ABSTRACT:
The Cartographic Institute of Catalonia (ICC) has acquired a DMC digital camera and has performed some first investigations regarding radiometric performance and geometric accuracy potential. In this cooperation with the Institute of Geodesy and Photogrammetry (IGP), ETH Zurich various aspects are analysed. The investigations make use of recent test flights near Tortosa, a plane region with varying landcover. For the quantitative analysis of the DMC results, a ground control points and lidar data exist, which have been simultaneously acquired with the DMC images. The first part of the investigations focusses on geometric sensor modeling and aerial triangulation. Preliminary results of ICC have shown that when standard additional parameters, like the 12 Ebner parameters, are used in AT, significant systematic errors remain and each of the 4 subimages that form the virtual panchromatic image has a different pattern of image deformations. In these investigations, we do not perform analysis of additional parameters in order to model these deformations, as this has been done in another ICC work. The results are analysed using GCPs established in the above mentioned testfield, using two different bundle adjustment programs.. Another part of our investigations regarding AT deals with automatic point transfer using a high quality multi-image, multi-primitive matching method developed at IGP, initially for automatic DSM generation. Different aspects like number, distribution and accuracy of the tie points are analysed, as well number of rays per tie point. The second part of the paper focuses on automatic DSM generation. Although digital cameras offer characteristics, like better image quality, that could be used favourably in automated DSM generation, almost all commercial systems employ matching methods with limitations, like no support of multi-image matching. In these investigations, we briefly introduce the above mentioned IGP multi-image matching and present the matching results. Initial results with other digital cameras and images with large forward and side overlap have shown that this matching approach can produce DSMs at least as dense as those produced by airborne laser scanning and almost as accurate, preserving also very well surface discontinuities. The processing and DSM control was performed by IGP using lidar data provided by ICC, while ICC made an independent control of the aerial triangulation using the software programs at ICC.

1. INTRODUCTION

Digital photogrammetric cameras of large format have been commercially introduced since 2000. Since then, their usage has steadily increased with currently over 100 systems sold, compared to about 1000 film cameras in use. These digital sensors are mainly, and almost equally, divided among the 3 main manufacturers: Leica (ADS40), Intergraph (DMC) and Vexcel (UltraCam-D). Some major aerial camera users, like national mapping agencies (e.g. in France and Sweden), have stopped using aerial film cameras and switched to fully digital image acquisition. In spite of this and the many promising characteristics of digital vs. film cameras, these new systems have been very poorly investigated. The great majority of the publications on them come from the manufacturers themselves, thus can not be considered objective. Users, especially private firms, hesitate (for obvious reasons) to report problems, and do not have the time and/or knowledge to perform in-depth analysis of their performance. Even the academic and research community has not provided significant analysis of their performance. Such an analysis is even more important as these systems are much more complicated optically, mechanically and electronically than the classical film cameras, and thus potentially less stable and subject to errors. In particular, large format cameras almost always use multiple linear or frame CCDs and thus have a much more complicated interior geometry, which requests for a new comprehensive sensor modeling and calibration. Furthermore, they often require, at least partially, different processing methods than the ones employed with film cameras. Not just because of their different sensor models but also in order to exploit their higher potential compared to film, like better radiometric quality and often higher image overlap. The lack of substantial scientific research on these systems is partly due to an insufficient understanding of their problems, the low availability of free and especially good-quality images, and the need of high-accuracy reference data and testfields which are hard to establish and maintain. Among the scarce non-manufacturer publications on these new systems, one could mention e.g. the overviews by Cramer (2005b, 2005c), including also results on ADS40, investigations on UltraCam-D by Honkavaara et al. (2005) and Honkavaara (2005), while investigations on DMC will be mentioned below. Specific aspects on calibration are treated by an EuroSDR working group on Digital Camera Calibration (EuroSDR, 2006), Cramer (2005a), and on calibration and georeferencing by Hofmann (2005).

The present work is motivated by the above problems and a long-time relationship between IGP and ICC, which uses DMC in their production. The technical specifications of DMC are given on www.intergraph.com, while additional information is given by manufacturer employees in Madani et al. (2004), Rosengarten (2005), Dörstel (2005) and Dörstel et al. (2005). Initial investigations by ICC have been reported by Alamús et al. (2005) and Kornus (2005), while Heuchel (2005) reports on

[1] Now with the Institute for Photogrammetry and Remote Sensing, Chinese Academy of Surveying and Mapping, Bejing, P.R.China.
[*] Corresponding author. http://www.photogrammetry.ethz.ch

AT and DSM generation results using DMC data, albeit without any reference data. The aims of this investigation were initially manifold, although some of them could not be yet realised due to time constraints. The first aim was to investigate a better sensor modelling due to image deformations in each of the 4 subimages of the DMC PAN cameras reported by Kornus (2005) and Cramer (2005c). The second aim was to investigate the potential of an automated DSM generation approach developed at IGP, which has better performance than commercial systems. The third one was to check the adaptation of this matching algorithm to automated tie point extraction for AT.

2. DATA

2.1 Image and lidar data

The image data consists of 28 DMC images with a ground sampling distance of 22 cm arranged in 4 parallel flight strips in E/W direction of 7 images each. They cover a small area of about 5km x 5km size located close to the Ebro delta south-west of Barcelona with variable land cover. The images are taken from a large test dataset collected in December 2005 with the goal to check and verify the performance of a second DMC, which the ICC is planning to purchase in 2006. DMC images were acquired together with lidar data from 2.500m altitude (1:21,000 scale factor). The forward and side overlap of the DMC images was 60% and 75%. This high side overlap and the presence of simultaneously collected lidar data were the major reasons to choose the data from this flight for the present study.
The lidar system used was an Optech 3030. There are some gaps in the data due to water surfaces and low reflectance objects (there are rice fields, possibly flooded, in the region). The lidar accuracy given by Optech is flying height divided by 2000 in planimetry and 30 cm in height at 2300m flying altitude. The practical experience of ICC is about 50% better, i.e. from 2300m about 50cm in planimetry and better than 15cm in height. The lidar data consisted of 4 strips (the 4th strip flown twice due to clouds) and two cross strips at 45 and 90 deg, which are used for in-flight calibration, since the calibration data of the lidar system is not that stable. This calibration however takes more care parameters affecting the height (like roll angle or scanner scale) rather than the planimetry, so it is quite possible, that the data is affected by a pitch error, influencing the X direction.

2.2 Ground control points

From the ground control point (GCP) network, established for the DMC test, only 4 points were located in the selected area. Additional 13 GCPs were recovered from earlier ICC flights taken between 2000 and 2004 in image scales 1:5.000 and 1:30.000. The difference in time and image scale posed considerable problems in point identification, i.e. from the 17 points only 11 GCP could be identified in the DMC images. 2 points originate from image scale 1:30.000 with an accuracy of 25 cm in X, Y, Z (labeled GCP_25/25 in Table 1 and Fig. 1), and 9 points from image scale 1:5.000 with an accuracy of 5 cm in X, Y and Z. The points were manually identified in one image with pixel accuracy and later automatically correlated. The distribution of the points is shown in Fig. 1. Due to the limited identification accuracy and assuming that identification errors influence mainly the planimetry, these 9 points were introduced into the bundle adjustment with a higher horizontal a priori standard deviation of 20 cm in X and Y (1 pixel), and 5 cm in Z (labeled GCP_20/05). The image coordinates of the GCPs were introduced with 6.0 microns (0.5 pixel).

3. AERIAL TRIANGULATION AND BUNDLE ADJUSTMENT

3.1 GPS data

GPS data were registered simultaneously with the DMC images, but turned out to be desynchronized by 45 ms. The error was corrected during trajectory calculation, which resulted in a reduced accuracy of the GPS observations, especially in X (flight direction). The GPS observations were introduced into the bundle adjustment with an a priori standard deviation of approximately 25 cm in X, and 3 cm in Y and Z.

3.2 Tie points and bundle adjustment with Pat-B

Along with the GCP measurements, a regular distributed network of tie points was generated, most of them with pixel accuracy. The latter can not be explained yet, as the applied matching algorithm provides subpixel results. They have been determined by an automatic tie point extraction which is under development in the IGP program Sat-PP (see Section 4). The matching is a modification of the procedure explained in Section 4. The tie points were homogeneously distributed. Only 17.3% and 13.6% of the points had 2 and 3 rays, respectively, the rest had 4-12 rays. The results included some blunders, which were excluded partly manually, and partly in the blunder detection of Pat-B. The remaining number of tie points was 422. The tie point the GCP observations were introduced into Pat-B without using GPS and IMU observations and no self-calibration. The sigma a posteriori was 7.3 microns (0.6 pixels). The mean standard deviations of the exterior orientation were (in m and gon): X 0.36, Y 0.43, Z 0.23, ω 0.013, ϕ 0.014, κ 0.007. The mean standard deviations of the object coordinates (in m) were: X 0.36, Y 0.43, Z 0.23.
In order to produce tie points of higher accuracy, the data was imported into the commercial aerial triangulation software Match-AT of Inpho (Sigle and Heuchel, 2001), while the already existing tie points served as initial positions for tie point search areas. The program yielded 2771 new tie points. The estimated sigma naught was 1.6 micron (0.13 pixel). Similar results using DMC images and Match-AT are reported by Heuchel (2005). Nevertheless, these 2771 tie points were introduced into the bundle adjustment also with low weight, i.e. an a priori standard deviation of 6.0 micron. The reason is given in the next section. The 422 tie points of lower accuracy have not been further used.

3.3 Bundle adjustment with ACX

The DMC virtual images are generated by the Intergraph software by the following procedure. First a radiometric balancing of the 4 subimages is performed. Then, each subimage is corrected for lens distortion, using laboratory calibration values. Matching in the overlap regions of the 4 subimages leads to tie points which are used in a photogrammetric bundle adjustment to determine ω and ϕ parameters for each subimage (the other exterior orientation parameters are highly correlated) and then the 4 subimages are stitched to the virtual image, which is a projection (rectification) on a plane at the average height of the scene. The multispectral images are rectified to the same plane and then a pansharpening process generates the final images. In the above processes, several errors may remain. Some interior orientation

errors of each subimage may remain unmodelled and/or the laboratory calibration values may be not valid anymore. X, Y, Z and k values of each subimage may have changed. The planar rectification causes pixel shifts, which depend on the flying height over terrain and the height range of the scene. The pansharpening causes additionally edge smoothing and artifacts (which were not an influence in this case as the PAN images were used).

Comprehensive investigations at the ICC on aerial triangulation accuracy with DMC images showed that the bundle adjustment requires an appropriate self-calibration model, which takes into account the special 4 camera head geometry of the PAN DMC sensors, i.e. a separate set of block-invariant additional parameters (APs) must be applied to each image quadrant (Alamús et al., 2006). The use of no self-calibration or the standard approach of one common set of APs for the entire image might lead to a poor determination of the point heights in the block center, especially if no accurate GPS observations are available and the number, distribution or accuracy of the GCPs is not sufficient.

The bundle block adjustment was carried out with the ACX/GeoTex software developed at the ICC (Colomina et al., 1992). In order to be compatible with the DSM generation program Sat-PP (see Section 4), which up to now does not include APs for each DMC subimage, the bundle adjustment was calculated without APs. According to the results presented in (Alamús et al. 2006), a DMC block can also be well determined in the absence of appropriate self-calibration, if highly accurate GPS observations are available and the photogrammetric observations are introduced with low weight. In this case, the image distortions will be mainly expressed in the residuals of the photogrammetric observations and will not significantly affect the determination of the orientation.

From the 11 GCPs, 10 points were entered as full control points with the above given standard deviations. Due to the poor distribution and the reduced horizontal accuracy of the GCPs only 1 point was selected as independent check point. The residuals are plotted in Fig. 1 and the RMS values are listed in Table 1. They clearly demonstrate the low resulting horizontal accuracy caused by the poor image measurement accuracy of the GCPs. Due to the presence of highly accurate vertical GPS observations, the height accuracy is acceptable as indicated by the height residuals of the 8 higher weighted GCP_20/05 and the check point, although a single check point of course cannot be considered as representative.

The mean standard deviations of the exterior orientation were (in m and sec): X 0.06, Y 0.07, Z 0.05, ω 0.16, ϕ 0.12, κ 0.09. The mean standard deviations of the object coordinates (in m) were: X 0.04, Y 0.05, Z 0.10. The orientation results from Pat-B had differences in the left block part, especially at the upper half (see also residual differences in Fig. 7). The results of ACX are expected to be more accurate than those of Pat-B, due to more and more accurate tie points and integration of GPS observations, which improve the results especially in height.

	2 GCP_25/25	8 GCP_20/05	1 Check Point
RMS-X [cm]	34.3	19.9	-38.6
RMS-Y [cm]	10.5	27.6	11.4
RMS-Z [cm]	12.6	3.4	0.6

Table 1. Root mean square residuals at the control and check points.

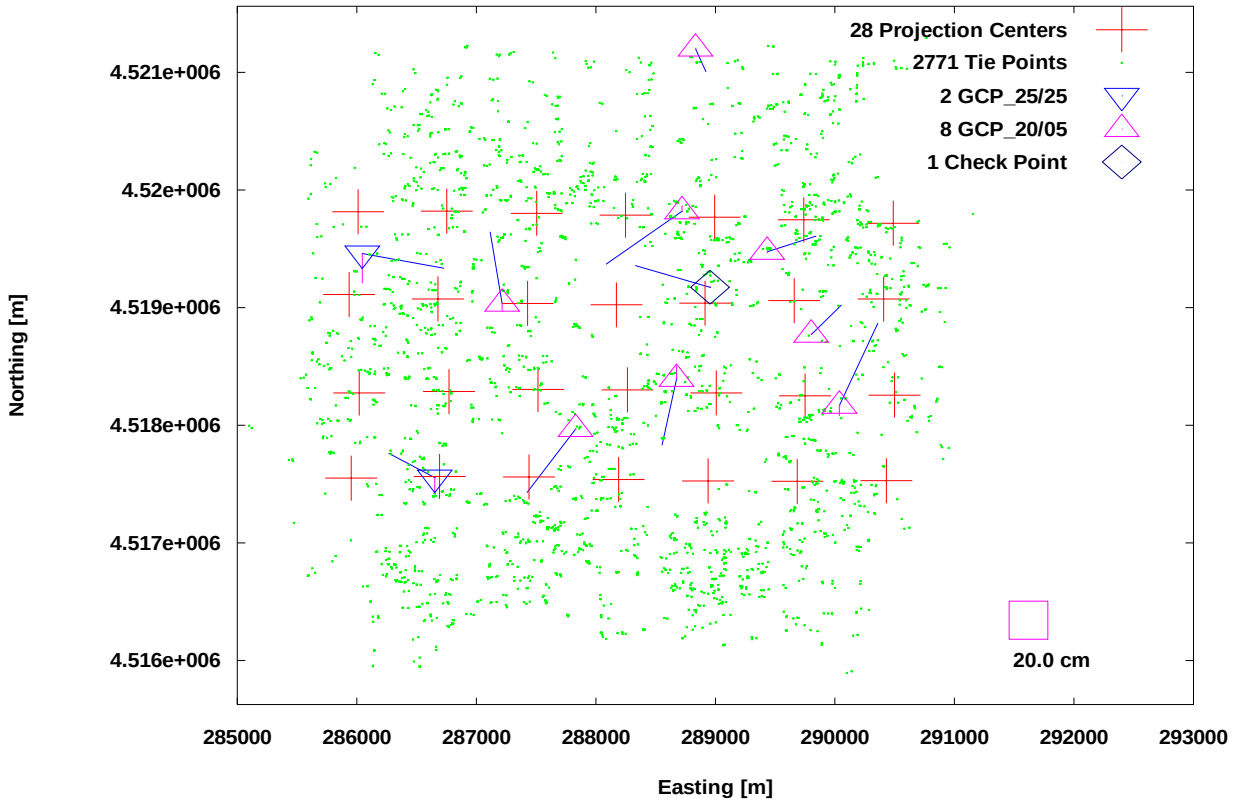

Figure 1. Point distribution and residuals of the control and check points.

4. DSM GENERATION METHOD

The automated DSM generation was performed using the Sat-PP program. Its matching algorithm is described in Zhang and Gruen (2004) and especially Zhang (2005), where details can be found. Here, only a brief summary of the method will be given.

In order to achieve successful and reliable matching, the method matches a dense pattern of features with an appropriate matching strategy, making use of all available and explicit knowledge, concerning sensor model, network structure, image content and geometrical constraints such as the epipolar geometry constraint. The approach combines area-based matching (ABM) and feature-based matching (FBM), matching parameter self-tuning, generation of more redundant matches and a coarse-to-fine hierarchical matching strategy.

The approach essentially consists of 3 mutually connected components: the image preprocessing, the multiple primitive multi-image (MPM) matching and the refined matching procedure. The overall dataflow is shown schematically in Fig. 2. The images and the given or previously estimated orientation elements are used as input.

The method has been applied to different kinds of images from different sensors (including high-resolution satellite system, traditional aerial photographs and digital aerial images) with varying surface relief and image content. It has been previously used with other DMC, as well as UltraCam-D, images however without reference DSM data. The fact that with digital cameras in many projects, especially in urban areas, high forward and side image overlap is used, provides additional advantages for this matching method, as it can match simultaneously any number of images (up to 13 with UltraCam-D), increasing thus completeness, accuracy and reliability of the results.

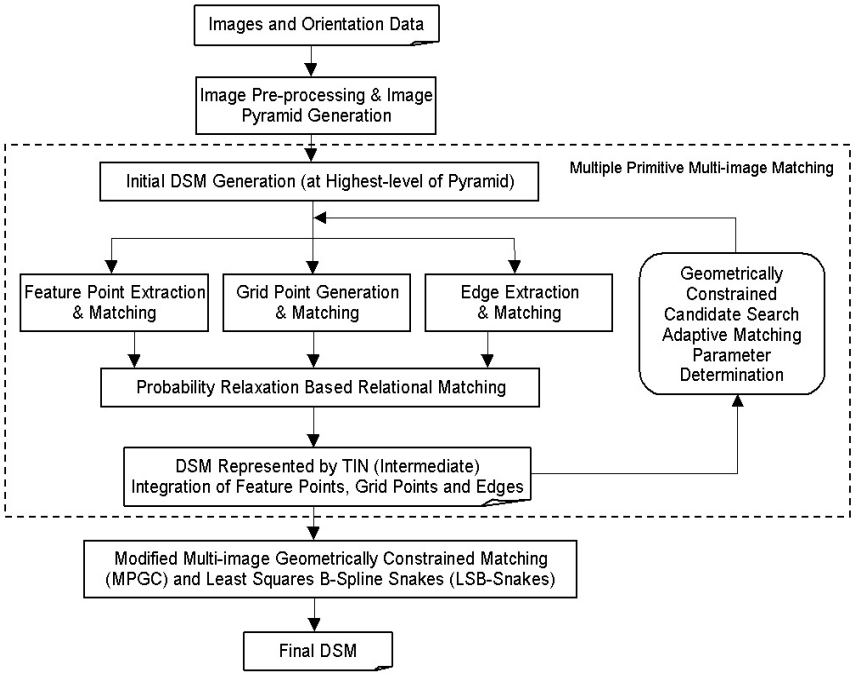

Figure 2. Workflow of the automated DSM generation approach.

4.1 Image preprocessing

In order to reduce the effects of the radiometric problems such as strong bright and dark regions and to optimize the images for subsequent feature extraction and image matching, a pre-processing method, which combines an adaptive smoothing filter and the Wallis filter, was developed. Firstly, an adaptive smoothing filter is applied to reduce the noise level and to sharpen edges and preserve even fine detail such as corners and line end-points. Next, the Wallis filter is applied to enhance and sharpen the already existing texture patterns.

After the image preprocessing, the image pyramid is generated starting from the original resolution images. Three additional pyramid levels are generated, each with a reduced resolution by factor 3 from the previous level.

4.2 Multiple Primitive Multi-Image matching

The MPM matching procedure is the core of the developed approach for accurate and robust DSM reconstruction. Results from this approach can be used as approximations for the refined matching procedure with least squares matching methods. In the MPM approach, the matching is performed with the aid of multiple images (two or more), incorporating multiple matching primitives – feature points, grid points and edges, integrating local and global image information and utilizing a coarse-to-fine hierarchical matching strategy. The MPM approach consists mainly of 3 integrated subsystems: the feature point extraction and matching procedure, the edge extraction and matching procedure and the relaxation based relational matching procedure of grid points. Thus, it combines all essential image primitives for matching. The matching criterion used is based on modified normalised cross-correlation, providing subpixel accuracy and uses one image, usually the most nadir one, as the reference image. The modifications of cross-correlation consist of 3 parts: a) geometric epipolar constraints are used and the image spaces are connected via the object space coordinates of each point; b) the matching patch in the reference image is projected on the surface, estimated from the previous pyramid level, and

backprojected in the search images, thus shaping differences (scales, rotations etc.) between the matching patches can be accommodated; c) the computed cross-correlation is the sum of the cross-correlation between reference image and each remaining image, helping thus in the reduction of mismatches due to multiple solutions, occlusions etc.

4.3 Matching through image pyramids

The MPM matching approach starts with an initial matching at the lowest resolution pyramid level. At each pyramid level, an intermediate terrain surface is reconstructed from the mass points and edges. It is modelled by the triangular irregular network (TIN) using a 2D constrained Delaunay triangulation method. This TIN-form intermediate surface model in turn is used in the subsequent pyramid levels for providing the approximations and adaptively computing the matching parameters. Thus, while the matching procedure is going through the image pyramids, the surface model computed from the higher level of the image pyramid is successively refined at the lower level and finally, the dense and accurate surface model is reconstructed.
At each pyramid level, an automatic blunder detection procedure is performed in order to delete some mismatches.

4.4 Least squares approach to refined matching

Least squares matching methods are used in our approach to achieve slightly higher accuracy results for all matched features and for the identification of some false matches. For this, a modified MultiPhoto Geometrically Constrained Matching (MPGC) algorithm is used. The MPGC combines grey level matching with geometrical constraints derived from multiple image ray intersection conditions and a priori knowledge about the image orientation elements (Baltsavias 1991). It permits a simultaneous determination of pixel and object coordinates and allows for simultaneous matching with any number of images.
In order to process linear array images, the standard MPGC algorithm is extended by integrating the geometric constraints derived from the linear array sensor models. In addition, we follow the algorithms proposed by Li (1997) and implement a simplified version of the Least Squares B-Spline Snakes (LSB-Snakes) to match the edges, which are represented by parametric linear B-spline functions in object space. LSB-Snakes can be seen as an extension of the standard MPGC algorithm. With this method, the parameters of linear B-spline functions of the edges in object space are directly estimated, together with the matching parameters in the multiple images.
After matching finishes, with or without use of the modified MPGC, a regular grid is interpolated with a user-defined grid spacing, and from this grid a colour-coded image is generated for visual inspection. The density of the matched features is very high, with an average point density of about 3 pixels. To have a redundancy and generate a better quality grid, the grid spacing is usually selected as 5 times the ground pixel size.

5. DSM RESULTS AND ANALYSIS

Two DSMs were produced by matching, using the orientation from Pat-B and ACX respectively, covering an area of 5.1 (E/W) by 5.7 (N/S) km. The 1m grid generated DSM using the ACX orientation is presented in Fig. 3. Figs. 4 and 5 are zoom-ins that show that the DSM has good quality and high resolution. Building roofs are well modeled, as well as other terrain discontinuities. The same applies to trees, bushes and even fine structures in the fields. White shows water areas that have been masked out manually before matching. The density of the matching DSM is, in this case, better than the density of the laser data. This is generally the case, i.e. with matching of digital images, a DSM with equal or higher density than a laser DSM can be generated. The used matching method provides similar results to laser, even regarding accuracy. For comparison with laser, the first pulse of the unfiltered laser data was used. The average point density of the laser data was 1.2 points/m^2. However, in vegetation areas (and there are quite many in this test site) the laser beam often measures below the top surface, thus leading to differences with the matching DSM, which do not consist errors of the latter.
For quality evaluation of DSMs, often a reference DSM is interpolated in the DSM to be checked. This approach is suboptimal, since a) at surface discontinuities surface modeling errors may lead to large height differences although the measurements are correct, and b) if the reference frames of the two DSMs differ (e.g. shifts and tilts), then again large differences occur, especially at discontinuities although the heights may be correct. The first shortcoming can be overcome by the approach used in Poli et al. (2004), where the shortest 3D distance between each reference point and the produced DSM is used. To avoid also the second shortcoming we used the approach of Gruen and Akca (2005) and the respective semi-commercial program LS3D. This method performs 3D least squares matching to match a 3D point cloud (slave) to a master point cloud, possibly with different point density and accuracy. The slave 3D point cloud is transformed by a 7-parameter 3D similarity transformation estimated by least squares by minimizing the sum of the squares of the 3D distances between the two point clouds. After the transformation of the slave point cloud, the standard deviation of the remaining distance differences is estimated (sigma-naught) as quality measure, and it is decomposed in X, Y and Z components. The residuals can also be decomposed in X, Y, Z components.
Figure 6 shows the coverage of the DSMs. The two lidar DSMs were interpolated regular grids. The 7-strip lidar DSM had 22 milion points and could not be processed by the LS3D program (see below). Thus, the grid spacing was reduced from 1m to 2m. The red lidar DSM had a grid spacing of 1 m.

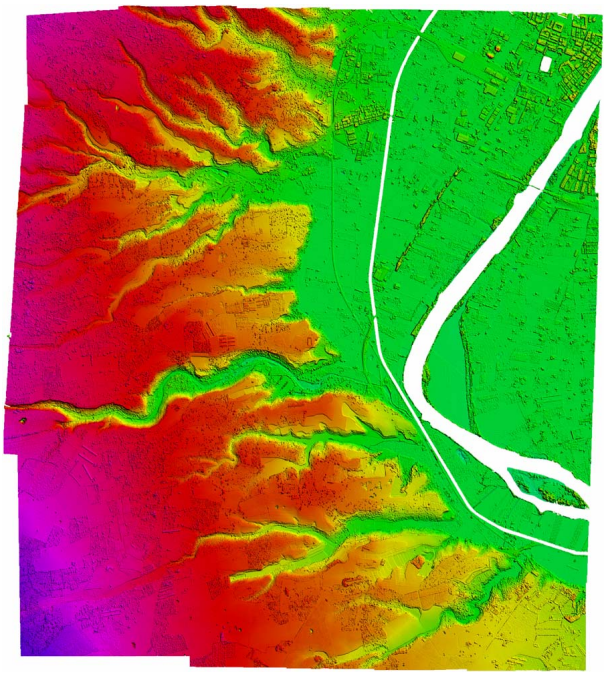

Figure 3. The 1m grid matching DSM using ACX orientation.

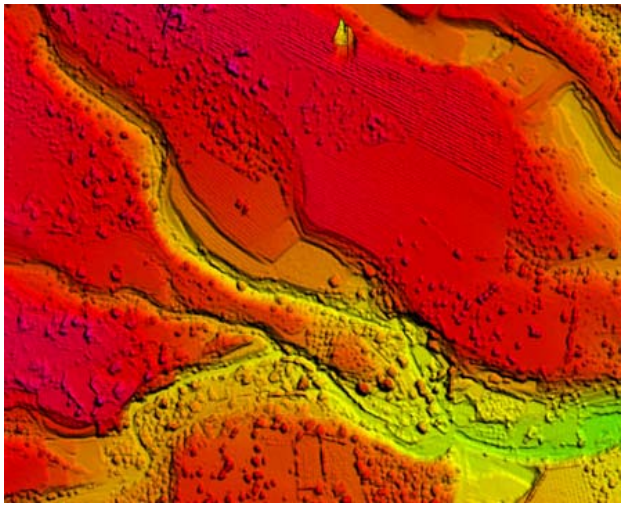

Figure 4. Zoom-in of Fig. 3.

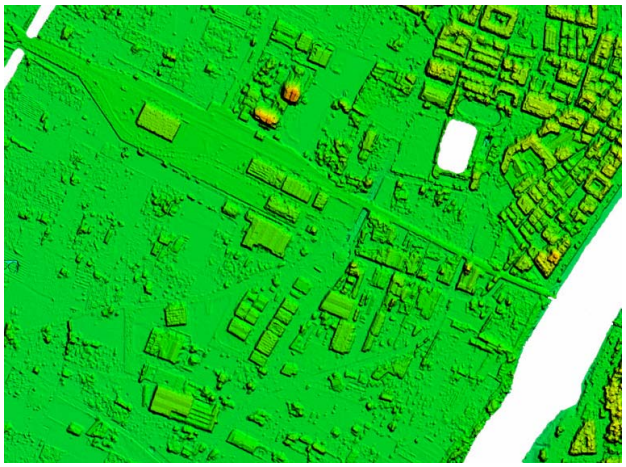

Figure 5. Zoom-in of Fig. 3.

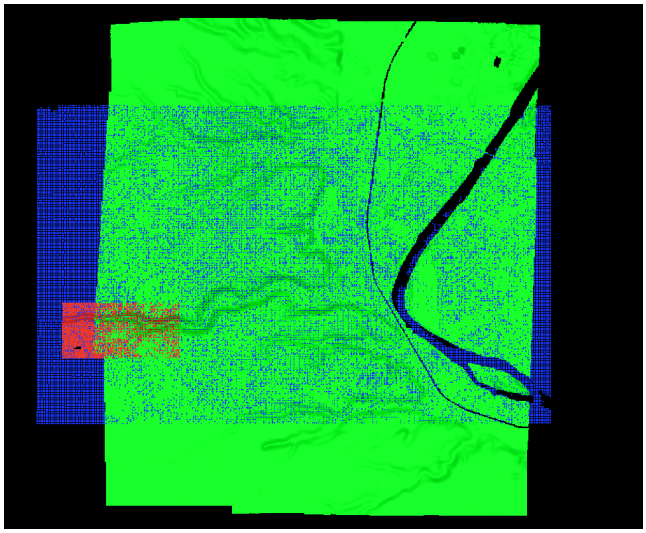

Figure 6. DSM coverage. Green: matching DSM. Blue: Lidar DSM (7 strips). Red: Part of the 4-strip lidar DSM.

Table 2 shows the results of LS3D. After some preliminary test, it showed that only the translation of the 7-parameter transformation were significant. The results for the two orientations are very similar except for Tz in the 4-strip lidar area. The reason is that these numbers are global and are not influenced apparently significantly from local differences between the two orientations. The translation values represent the bias between the two DSMs. In planimetry, this bias is due to the different orientation of images and lidar, and is significant only in Y (N/S) direction. In height, bias is possible due to the same reason and additionally due to partial penetration of vegetation by the lidar data (note that the matching DSM is higher than the lidar heights, as the negative sign of Tz shows). The sigma a posteriori is the standard deviation of the 3D spatial differences (shown in Fig. 7) between slave and master DSMs after performing the translation. Its decomposition in X, Y, Z components is shown in Table 3. Again, there is no significant difference between the two image orientations. The X and Y values are similar and about 0.3 m, while in height it is about 0.65 m. This is actually the difference between the two DSMs after removing the systematic bias in X, Y and Z. The differences, as Fig. 7 shows, are higher at surface discontinuities, possibly also due to modeling errors. The high differences at upper right, and especially bottom left parts, may be due to errors in the lidar data.

6. CONCLUSIONS

Due to time constraints, the GCP point measurement was suboptimal. GCPs well-defined in the images could have been measured by GPS in the field, providing a dense enough network of control and check points. This would allow a better orientation and more accurate matching DSM and a better control of the bundle adjustment results. Also the density, and to a certain extent the accuracy of the lidar DSM was not sufficient. Since matching DSMs can be very dense, the reference DSM should be 2-3 times denser. In spite of these, the achieved standard deviation of the height differences was about 0.65m. With a better orientation, usage of APs in the bundle adjustment and DSM generation and without the differences due to vegetation penetration, we expect this difference to drop quite below 0.5 m.

The automatic tie point measurement in Sat-PP can be denser without any problem. Improvements are needed in achieving subpixel accuracy and reducing the number of blunders by automatic quality control. We will report further developments in the future.

REFERENCES

Alamús, R., Kornus, W., Palà, V., Pérez, F., Arbiol, R., Bonet, R., Costa, J., Hernández, J., Marimon, J., Ortiz, M.A., Palma, E., Pla, M., Racero, S., Talaya, J., 2005. Validation Process of the ICC Digital Camera. Proc. ISPRS Workshop "High-Resolution Earth Imaging for Geospatial Information", 17-20 May, Hannover, Germany, on CD-ROM. Available at http://www.ipi.uni-hannover.de/html/publikationen/2005/workshop/contents_a-z.htm (accessed 5 June 2006).

Alamús R., Kornus W., Talaya J., 2006. Studies on DMC geometry. ISPRS Journal of Photogrammetry and Remote Sensing, Theme Issue “Digital Aerial Cameras”, in print.

Baltsavias, E. P., 1991. Multiphoto Geometrically Constrained Matching. Ph.D. Dissertation, Report No. 49, Institute of Geodesy and Photogrammetry, ETH Zurich, Switzerland.

Colomina, I., Navarro, J., Termens, A., 1992: GeoTeX: A general point determination system. In: International Archives of Photogrammetry and Remote Sensing, Vol. 29, Part B2, pp. 656-664.

Cramer, M., 2005a. Digital camera calibration and validation. GeoInformatics, 8(3): 16-19.

Cramer, M., 2005b. Digital Airborne Cameras- Status and Future Proc. ISPRS Workshop "High-Resolution Earth Imaging for Geospatial Information", 17-20 May, Hannover, Germany, on CD-ROM. Available at http://www.ipi.uni-hannover.de/html/publikationen/2005/workshop/contents_a-z.htm (accessed 5 June 2006).

Cramer, M., 2005c. Digital airborne cameras – status and future Presentation at SGPBF Workshop 'Digital Aerial Cameras – Experiences and methodological Developments', EPFL Lausanne, 25. November 2005 http://www.sgpbf.ch/de/mitteilungen.html (accessed 5 June 2006).

Dörstel, C., 2005. DMC – PPS and new Features. Proc. ISPRS Workshop "High-Resolution Earth Imaging for Geospatial Information", 17-20 May, Hannover, Germany, on CD-ROM. Available at http://www.ipi.uni-hannover.de/html/publikationen/2005/workshop/contents_a-z.htm (accessed 5 June 2006).

Dörstel C., Traub S., Wuescher D., 2005. Towards fully automated processing of DMC images. Proc. ISPRS Workshop "High-Resolution Earth Imaging for Geospatial Information", 17-20 May, Hannover, Germany, on CD-ROM. Available at http://www.ipi.uni-hannover.de/html/publikationen/2005/workshop/contents_a-z.htm (accessed 5 June 2006).

EuroSDR, 2006. Digital Camera Calibration EuroSDR Working Group WEB page. http://www.ifp.uni-stuttgart.de/eurosdr/index.html (accessed 5 June 2006).

Gruen, A., Akca, D., 2005. Least squares 3D surface and curve matching. ISPRS Journal of Photogrammetry and Remote Sensing, 59 (3): 151-174.

Heuchel, T., 2005. Experience in Applying Matching Techniques Using Images from Digital Cameras. Photogrammetric Week '05, D. Fritsch (Ed.), available at http://www.ifp.uni-stuttgart.de/publications/phowo05/phowo05.htm (accessed 5 June 2006).

Hofmann, O., 2005. Calibration and Georeferencing of Aerial Digital Cameras. Photogrammetric Week '05, D. Fritsch (Ed.), available at http://www.ifp.uni-stuttgart.de/publications/phowo05/phowo05.htm (accessed 5 June 2006).

Honkavaara, E., 2005. Testing digital camera systems in permanent Sjokulla testfield – results from UltraCamD tests. Presentation at SGPBF Workshop 'Digital Aerial Cameras – Experiences and methodological Developments', EPFL Lausanne, 25 November, available at http://www.sgpbf.ch/de/mitteilungen.html (accessed 5 June 2006).

Honkavaara, E., Markelin, L., Ilves, R., Savolainen, P., Vilhomaa, J., Ahokas, E., Jaakkola, J., Kaartinen, H., 2005. In-Flight Performance Evaluation of Digital Photogrammetric Sensors Proc. ISPRS Workshop "High-Resolution Earth Imaging for Geospatial Information", 17-20 May, Hannover, Germany, on CD-ROM. Available at http://www.ipi.uni-hannover.de/html/publikationen/2005/workshop/contents_a-z.htm (accessed 5 June 2006).

Kornus, W., 2005. Tests and performance analysis of DMC at the Cartographic Institute of Catalonia (ICC). Presentation at SGPBF Workshop 'Digital Aerial Cameras – Experiences and methodological Developments', EPFL Lausanne, 25 November, available at http://www.sgpbf.ch/de/mitteilungen.html (accessed 5 June 2006).

Li, H., 1997. Semi-automatic Road Extraction from Satellite and Aerial Images. Ph. D. Dissertation, Report No. 61, Institute of Geodesy and Photogrammetry, ETH Zurich, Switzerland.

Madani, M., Dörstel C., Heipke C., Jacobsen K., 2004. DMC practical experience and accuracy ssessment. In: International Archives of Photogrammetry, Remote Sensing and Spatial Information Sciences, Vol. 35, Part B2 (and on DVD). Available at http://www.isprs.org/istanbul2004/comm2/papers/162.pdf (accessed 5 June 2006).

Poli, D., Zhang, L., Gruen, A., 2004. SPOT-5/HRS stereo images orientation and automated DSM generation. In: International Archives of Photogrammetry, Remote Sensing and Spatial Information Sciences, Vol. 35, Part B1, pp.421-432 (and on DVD). Available at http://www.isprs.org/HRS/PDF/77.pdf (accessed 5 June 2006).

Rosengarten, H., 2005. The DMC Solution Proc. ISPRS Workshop "High-Resolution Earth Imaging for Geospatial Information", 17-20 May, Hannover, Germany, on CD-ROM. Available at http://www.ipi.uni-hannover.de/html/publikationen/2005/workshop/contents_a-z.htm (accessed 5 June 2006).

Sigle, M., Heuchel, T., 2001. MATCH-AT: Recent Developments and Performance. Photogrammetric Week 2001, Wichmann Verlag.

Zhang, L., 2005. Automatic Digital Surface Model (DSM) Generation from Linear Array Images. Ph. D. Dissertation, Institute of Geodesy and Photogrammetry, ETH Zurich, Switzerland, Report No. 88.

Zhang, L., Gruen, A., 2004. Automatic DSM Generation from Linear Array Imagery Data. IAPRS, Vol. 35(B3): 128-133.

Template surface	Search surface	# valid points in template surface	# used points in the LS3D matching	Iterations	Sigma a priori (m)	Sigma a posteriori (m)	Tx (m)	Ty (m)	Tz (m)
LID_7ST	DMC_PATB	5,252,411	4,250,745	3	0.96	0.80	-0.00	-0.64	-0.06
LID_7ST	DMC_ACX	5,252,411	4,248,776	3	0.95	0.79	+0.05	-0.62	-0.07
LID_4ST	DMC_PATB	844,734	605,319	3	1.09	0.90	-0.01	-0.37	-0.26
LID_4ST	DMC_ACX	844,734	604,945	3	1.07	0.90	+0.01	-0.39	-0.12

Table 2. The results of the LS3D program. The used poinrs are less because the overlap was not 100% and some points were additionally excluded. This was performed using a simple robust estimation by binary re-weighting according to sigma. In all experiments, correspondences whose Euclidean distance is greater than 10*Sigma are excluded and regarded as either outliers or occlusion. The a priori sigma is computed after an initial iteration.

Template surface	Search surface	**Sigma a posteriori (m)**	Decomposition of sigma a posteriori into components	**Std. deviation (m)**	Mean (m)	Min (m)	Max (m)
LID_7ST	DMC_PATB	**0.80**	X	**0.32**	0.00	-8.04	7.99
			Y	**0.31**	0.00	-7.55	7.72
			Z	**0.66**	0.00	-5.81	5.87
LID_7ST	DMC_ACX	**0.79**	X	**0.33**	0.00	-8.10	7.61
			Y	**0.31**	0.00	-7.57	7.46
			Z	**0.65**	0.00	-5.74	5.72
LID_4ST	DMC_PATB	**0.90**	X	**0.33**	0.00	-8.45	8.05
			Y	**0.40**	0.00	-8.40	7.71
			Z	**0.73**	0.00	-6.15	6.25
LID_4ST	DMC_ACX	**0.90**	X	**0.33**	0.00	-8.45	8.06
			Y	**0.41**	0.00	-8.24	8.54
			Z	**0.73**	0.00	-6.33	6.14

Table 3. Decomposition of values of Table 2 in X, Y and Z components.

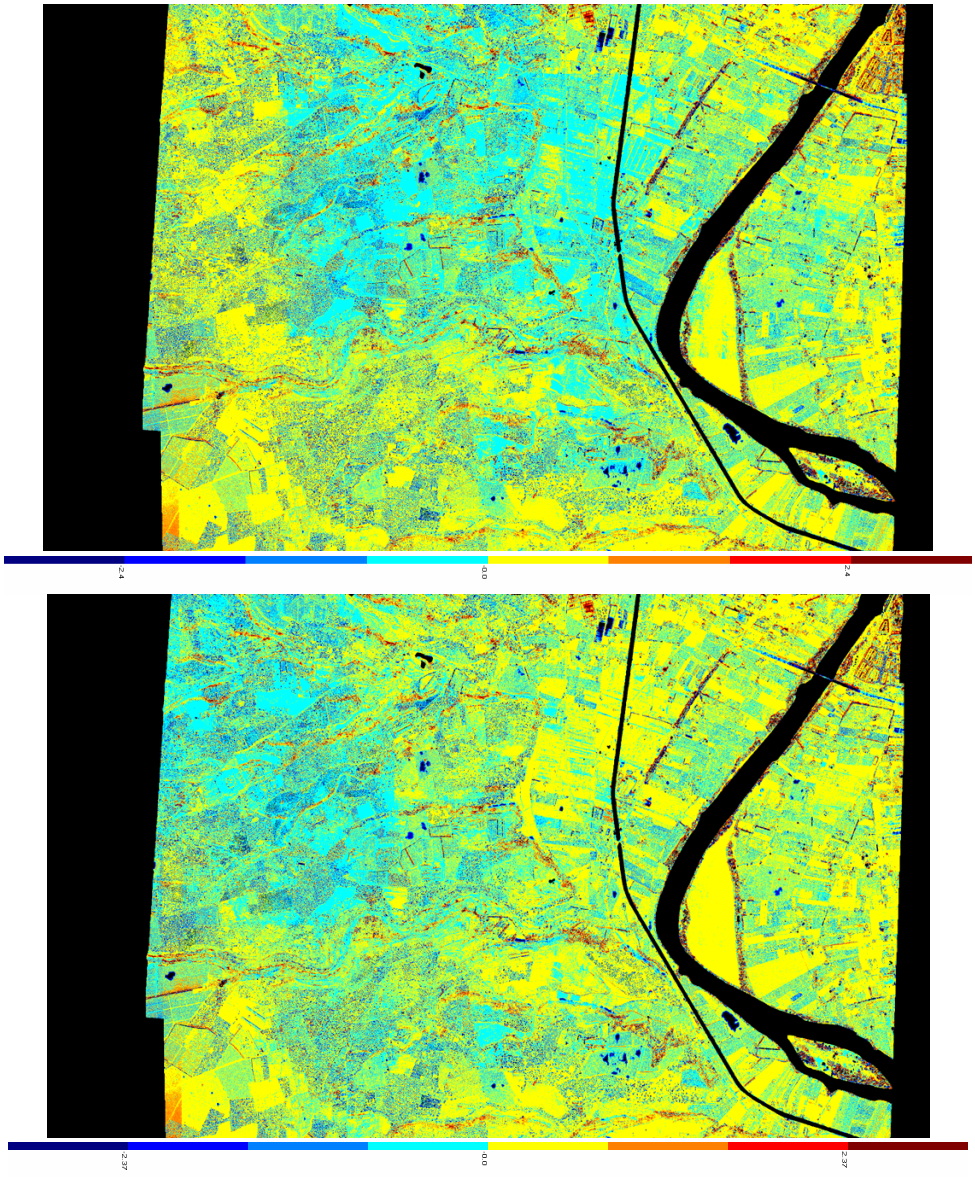

Figure 7. Residuals (3D spatial differences between master and slave DSMs) for Pat-B (top) and ACX (bottom) orientations. Note the residual differences in the upper left and central part, where the two orientations differed most.